STABILITY OF THE HALLEY COMETO-SHEATH WITH RESISTIVITY AND PLASMA MOTION

KRISHNA M. SRIVASTAVA, BRUCE 'I'. TSURUTANI,

BRUCE E. GOLDSTEIN, V. SHARMA*

(Jet Propulsion Laboratory, California Institute of Technology,

4800 Oak Grove Drive, Pasadena, CA 91 109)

* (Institute for Systems Studies and Analyses, Department of Defense

Research Development, Metcalfe House, Delhi-l 10 054, India)

Abstract

The MHD stability of the cometary inner sheath determined by the balance between the inward Lorentz body force and the outward ion-neutral drag force is investigated by numerically solving the wave equations which include resistivity, plasma motion and plasma pressure with the help of two-point boundary value method. The eigenvalues and the eigenfunctions are obtained numerically by treating the cometary inner sheath as a layer of finite thickness, bounded by the contact surface, i.e., the diamagnetic cavity boundary. To gain an insight into the problem, certain limiting cases of the wave equations are also discussed, The diamagnetic cavity boundary and the adjacent layer of about 100 km thickness of comet Halley is found to be unstable. The effects of finite plasma pressure, dissociative recombination, mass loading due to photoionization, resistivity, and plasma motion are found to be stabilizing but are unable to quench the instability completely. An estimate of τ_c/τ_i shows that it lies in the range 10 to 20 or even higher which appears to be sufficient for the effective penetration of the magnetic field perturbations into the cavity surface. Motion of the Halley ionopause has been confirmed by observations: according to Neubauer (1987), Halley ionopause seemed to have strong ripples with a wavelength of several hundred kilometers,

Subject Headings: Comets, Cometosheath, MHD Stability

I, INTRODUCTION:

Three categories of cometary boundaries have been identified according to the observations (Cravens, 1989): i) cometary dynamical boundries, ii) solar wind and IMF boundaries, and iii) transient boundaries, The dynamical boundaries are the permanent features of cometary plasma environment, The instruments on board the Giotto, Vega and ICE showed that the plasma in the inner coma of the comet Halley was almost stationary and of cometary origin. A field-free diamagnetic cavity deep within this stagnation region was encountered by the Giotto Spacecraft (Neubauer et al., 1986). The magnetic field dropped from 20 nT to nearly zero within a thin layer of about 25 km thickness. The magnetic field exhibited a maximum of about 50-60 nT thousands of kilometers away from the ionopause (cavity surface designated as CS) - 4600 km from the nucleus. The formation of such a field-free region has been explained by considering the balance between the inward Lorentz JxB body force and the outward ion-neutral drag force exerted on the plasma element (Ip and Axford 1982; Cravens, 1986; Ip and Axford 1987, 1990).

The stability of the cometary ionopause treated as tangential discontinuity interface was investigated for disturbances of wavelengths much greater than the ionopause thickness (Ershkovich and Mendis, 1986; Ershkovich et al., 1986). Ershkovich and Flammer (1 988) have shown that the finite amplitude effects can suppress the Kelvin -Helmholtz instability whereas the Rayleigh-Taylor and the drag instabilities persist. Ershkovich et al., (1989) and Mckenzie et

al., (1990) performed a stability analysis of the cometary ionosphere/i onopause of the comet Halley by using JWKB approximation and discussed certain limiting cases of the wave equations under the slow variation approximation of the equilibrium quantities. The ionopause boundary resulting from the balance between the ion-neutral friction and Lorentz body force was shown to be unstable. Inclusion of the effects of photoionization and dissociative recombination resulted in the stabilization of ionosphere except the Halley ionopause and adjacent ionospheric layer of about 100 km thickness. Numerical solutions of the MHD stability wave equations derived in Ershkovich et al., (1989) and McKenzie et al., (1 990) for the cometary ionosphere determined by the balance between the inward Lorentz body force and the outward ion-neutral drag force were obtained by using a two-point boundary value method (Srivastava et al., 1992). The eigenvalues and the eigenfunctions were obtained numerically by treating the cometary ionosphere as a layer of finite thickness, bounded by the diamagnetic cavity boundary. The magnetic field structure discovered in the ionosphere of comet Halley /Giacobini-Zinner was found to be unstable. The effects of finite plasma pressure, dissociative recombination and mass loading due to photoionization were found to be stabilizing, but were unable to quench the instability completely, i.e., the Halley ionopause and adjacent layer of about 1000 km thickness remained unstable. It was also found that the higher the neutral production rate the lesser was the growth rate for the instability. Ershkovich and Israelevich (1 992) have studied the effect of transverse plasma motion on the stability of the cometary

ionosphere and concluded that the instability might be convected downstream, The ionopause was shown to undergo convective instability,

In this paper, we study the stability of the cometo-sheath including the effects of plasma resistivity, plasma motion along the sun-comet line and plasma pressure, by considering the cometary sheath as a layer of finite thickness bounded by the ionopause on the inner side. The equations governing the stability are solved numerically for certain parameters for the comet Halley by using a two-point boundary value method. Although, the two-point boundary value method precludes the study of the stability of the critical layer of 25 km thickness due to the singularity of solutions as the magnetic field goes to zero at the ionopause, the present work is a step forward in that it presents numerical solutions and includes the effects of finite resistivity and radial plasma motion on the stability of the cometo-sheath which were not considered in previous papers (Ershkovich et al., 1989; McKenzie et al., 1990; Srivastava et al., 1992; Ershkovich and Israelevich, 1992). Certain limiting cases of the wave equations have also been discussed. We have obtained growth rates for disturbances of wavelengths ranging from 125 km to 2000 km. We have also est mated τ_c/τ_i where τ_c is the convection time for the perturbations to be convected well downstream and τ_i is the characteristic time for the amplitude to grow and found that it ranges from 1) to 20 or even higher which may be sufficient for the instability signatures to penetrate the boundary. The effects of photoionization, recombination, plasma pressure, and resistivity were

found stabilizing but the instability still persisted. The slow plasma motion included in the analysis resulted in the s abilization of the cometo-sheath s nce perturbations are convected downstream with the plasma bulk velocity before growing substantial ly.

The plan of the paper is as follows: In section 2 we formulate the linearized non-dimensional MHD equations suitable for numerical computation as a two-point boundary value problem. Approximate solutions of wave equations have been discussed in certain limiting cases in section 3. Results are described in section 4 and concluding remarks are given in section 5. Computational procedure has been described in Appendix A.

11. Formulation of the problem:

a). The Configuration:

We study the stability of a cometary ionospheric layer of about 1000 km thickness adjacent to and outside (he ionopause in the form of a slab, “the inner boundary being at the ionopause. The geometry considered is shown in Fig. (1c). Although the plasma in this layer is said to be stagnant, it is expected that there exists a very slow motion towards the ionopause (creeping motion). The MHD equations governing the evolution of physical quantities in a cometary ionosphere including plasma motion, resistivity, pressure, photoionization, and recombination are obtained by the normal procedure of linearizing the basic equations. The appropriate

continuity and momentum equations for a compressible plasma as derived in Ershkovich et al., (1989) are:

The continuity eqation:

$$\frac{\partial \rho}{\partial t} + \nabla \cdot (\rho \bar{U}) = \delta\rho_n - \frac{\alpha \rho^2}{M_i} \qquad (1)$$

The momentum equation:

$$\frac{d\bar{U}}{dt} = -\frac{1}{\rho} \nabla \left(P + \frac{B^2}{8\pi} \right) + \frac{\bar{B} \cdot \nabla \bar{B}}{4\pi\rho} + \nu_0 (U^* - \bar{U}) \qquad (2)$$

Here, ρ, $\bar{U}$, P, $\bar{B}$, $\bar{U}_n$, and M_i and denote, respectively, the plasma density, the velocity, the pressure, the magnetic field, the neutral gas velocity, and the mass of cometary ion. $V_* = v + \delta\rho_n/\rho$ is the ion neutral collision frequency enhanced by the mass loading. The terms $\delta\rho_n$ and $\alpha\rho^2/M_i$, represent, respectively, the photoionization rate and dissociation recombination rate.

The Faraday induction equation for a resistive plasma assuming that resistivity is uniform is given by:

$$\frac{\partial \bar{B}}{\partial t} = \nabla \times (\bar{U} \times \bar{B}) + \eta \nabla^2 \bar{B} \qquad (3)$$

Here, η denotes the resistivity of the plasma.

We derive the magnetic field structure by following Ip and Axford (1987) by neglecting the plasma inertia and pressure in the momentum equation. The balance between the magnetic stresses acting on the plasma element and the ion-neutral friction determines

the equilibrium structure of the magnetic field. The density is assumed to be inversely proportional to the distance from the nucleus and is taken as:

$$n_i = n_{i0} \; (r / L)^{rn} \tag{4}$$

where L is some radial scale length, r is the distance from the nucleus which coincides with x in the slab geometry, and m is the power index for the variation of plasma density.

The resulting structure of the magnetic field is given by (Ershkovich et al., 1989)

$$\frac{B_0}{B_m} = \left\{ \frac{2}{1+m} \left(\frac{r_m}{r}\right)^{1-m} - \frac{1-m}{1+m} \left(\frac{r_m}{r}\right)^{2} \right\}^{0.5}, \quad -1 < m < 1 \tag{5a}$$

$$\frac{B_0}{B_m} = \frac{r_m}{r} \left(1 + 2 \ln \left(\frac{r}{r_m}\right)\right)^{1/2}, \quad m = -1 \tag{5b}$$

where B_m denotes the maximum magnetic field at a distance r_m from the nucleus.

The magnetic field vanishes at a radial distance r0 from the nucleus given by

$$r_0 = r_m \left(\frac{1-m}{2}\right)^{1/(1+m)}, \quad m \neq -1 \tag{6a}$$

$$r_0 = r_m \exp(-1/2), \quad m = -1 \tag{6b}$$

The background plasma density ρ_0 is assumed to be determined by the photochemical equilibrium neglecting convection, i.e.,

$$\alpha \rho_0^2 / M_i = \delta \rho_n \tag{7}$$

where α is the dissociative recombination rate, δ is the photoionization rate, M_i is the ion mass of water group ions and p_n is the density of neutrals.

The equilibrium state is described by setting $\frac{\partial}{\partial t}$ to zero in equations (1) to (3). In particular, the stress balance equation (2) becomes:

$$U_0 \frac{dU_0}{dx} = -\frac{1}{\rho_0}\frac{dp_{t0}}{dx} + \left[\nu_0 (U_n - U_0) - \frac{V_{a0}^2}{R}\right] \tag{8}$$

where $p_{t0} = p_0 + B_0^2/8\pi$, $V_{a0}^2 = B_0^2/4\pi\rho_0$.

The third term on the right hand side represents the magnetic tension force in which $R = -\nabla B_0 / B_0$ is the radius of curvature of the lines of force. U_0 is in the negative x-direction and U_{J1} is in the positive x-direction.

The solution of the equilibrium Faraday equation gives:

$$U_0 = -(C - \eta / L_B) \tag{9}$$

where $L_B = \frac{dB_0}{dx} / B_0 = A/B$

$A = (2 \ln x + 1 - 2 \ln x_m)\, x$

$B = 2 (\ln x_m - \ln x)$

$C = \eta\, B/A$, with x replaced by x_1

$x_1 = x_o + \epsilon, \epsilon$ is taken as 10 to 20 km.

$x = r$ and $x_m = r_m$ in the slab geometry and U_O is negative outside the ionopause boundary. The thickness of the ionospheric layer whose stability we wish to investigate is very much smaller than the scale length of the magnetic field variations i.e. L_B is very large and can be taken to be uniform in this layer. Eq. (9) gives a small negative value of U_O which can be taken to be uniform in the first approximation, It is zero at x = I-O, the ionopause. In the numerical computation, the integration is performed from x = (x_1 + 1000) km to x = x_1 km to avoid the singularity at x = r_0 ($x_1 > r_0$) in the wave equations.

b). Wave Equations:

The stability analysis is made by taking a planar geometry shown in Fig, (1c). The equilibrium magnetic field is assumed to lie along the z-axis (perpendicular to the radial direction assumed to coincide with x -axis in planar geometry) which varies in the x-direction. The neutral gas and the plasma flow along the x-direction. The perturbed variables are:

$$\rho_1 = \rho - \rho_0 , \quad \bar{B}_1 = \bar{B} - \bar{B}_0 , \quad p_m \cdot \frac{\bar{B}_0 \cdot \bar{B}_1}{4\pi} ,$$

$$p = P - P_0 \qquad \bar{u} = \bar{U} - \bar{U}_0 = (U, v, w) \qquad (10)$$

which denote, respectively, the perturbations in density, magnetic pressure, plasma pressure, and plasma velocity.

The stability analysis is restricted to twist-free magnetic field perturbation i.e, $\bar{B}.\text{grad}\bar{B}$ is neglected. Following the usual procedure for the derivation of the linearized stability equations, we arrive at the following wave equations:

$$\frac{\partial \rho_1}{\partial t} + \nabla.(\rho_0 \bar{u}) = -\beta \rho_1 \tag{11}$$

$$\left(\left(\frac{\partial}{\partial t} + \nu_0\right)(\rho_0 \bar{u}) = -\nabla (p + p_m) + \left(g\rho_1 - \frac{2p_m}{R} - U_0 \nu_0 \rho_1\right)\hat{x}\right. \tag{12}$$

$$\frac{\partial p_m}{\partial t} + u\frac{dP_{m0}}{dx} + U_0\frac{\partial p_m}{\partial x} = V_a^2\left(\frac{\partial \rho_1}{\partial t} + u\frac{d\rho_0}{dx} + \beta\rho_1 + U_0\frac{\partial \rho_1}{\partial x}\right) + \eta\nabla^2 p_m \tag{13}$$

$$g = \nu U_n \ , \quad \beta = 2\alpha\rho_0 / M_i \ , \quad p_m = \frac{B_0 \ . \ B_1}{4\pi} \tag{14}$$

$\hat{x}$ is the unit vector along x-axis ,

Equation (13) can be rewritten in the form

$$\left(\frac{\partial}{\partial t} + \beta + U_0\frac{\partial}{\partial x}\right)\rho_1 = \frac{1}{V_a^2}\left(\frac{\partial}{\partial t} + U_0\frac{\partial}{\partial x} - \eta\nabla^2\right)p_m - \frac{N^2}{g}q \tag{15}$$

where $q = \rho_0 u$, $\nabla^2 \frac{\partial^2}{\partial \bar{x}^2} + \frac{\partial^2}{\partial y^2} + \frac{\partial^2}{\partial \bar{z}^2}$,

$$\text{and} \quad \frac{N^2}{g} = \frac{1}{\rho_0}\frac{d\rho_0}{dx} - \frac{1}{B_0}\frac{dB_0}{dx} \qquad (16)$$

The quantity N^2 is the MHD analogue of the square of the Brunt-Vaisala frequency (Brunt, 1941) and is a function of x. It plays a crucial role in the pointwise/local stability analysis of the system.

Taking divergence of Eq. (12) and making use of continuity equation (11), we obtain

$$\left(\nabla^2 + \frac{2}{R}\frac{\partial}{\partial x} + \frac{\partial}{\partial x}\left(\frac{2}{R}\right)\right) \rho_m = \left(\frac{\partial}{\partial t} + \nu_0\right) \times \left(\frac{\partial}{\partial t} + \beta + U_0\frac{\partial}{\partial x}\right)\rho_1 + \left(g\frac{\partial}{\partial x} - \nu_0 U_0 \frac{\partial}{\partial x} - c_0^2 \nabla^2\right)\rho_1 \qquad (17)$$

where

$$c_0^2 = \gamma p_{g0} / \rho_0 = \frac{T_0}{M_i}, \quad \text{for } \gamma = 1 \text{ and } \rho_{go} = n_{i0} T_0$$

For the sake of simplicity, the plasma pressure is assumed to be isotropic and the cometosheath to be isothermal. Although there is no rigorous justification for assuming isotropic and isothermal, a major motivating factor is that when the same assumption is made in the ideal MHD theory, the main features of MHD equilibrium and stability theory (sound waves, Alfven waves, kink and interchange

instabilities, "frozen in" heorem) remain qualitatively una tered (Hasam and Huba, 1987).

The x-component of Eq. (12) gives the per urbation in dens :y in terms of p_m and q:

$$(9 \quad U_0\nu_0 - c_0^2 \frac{\partial}{\partial x})\rho_1 = (\frac{\partial}{\partial x} + (2/R))p_m + (\frac{\partial}{\partial t} + \nu_0)\, q \qquad (18)$$

Equations (15), (17), and (18) constitute the system of wave equations governing the stability of the cometary inner sheath, In general, the equilibrium quantities are functions of x and the various operators do not commute. The wave equations are, therefore, solved numerically as an eigenvalue problem by using a two-point boundary value method. After eliminating q and performing a normal mode analysis by assuming that all perturbations vary as $f(x,y,t) = f^*(x)\ \exp(i\,(k_x x + k_y y - \omega t))$, the non-dimensional form of the wave equations can be written as:

$$D^2\rho_1^* = a_{21}\rho_1^* + a_{22}\, D\rho_1^* + a_{23}\, p_m^* + a_{24}\, Dp_m^* \qquad (19)$$

$$D^2 p_m^* = a_{41}\, \rho_1^* + a_{42}\, D\rho_1^* + a_{43}\, p_m^* + a_{44}\, Dp_m^* \qquad (20)$$

Here, $D = \frac{d}{dx}$ and the coefficients a_{ij} are given in appendix B. The non-dimensional quantities are

$$\rho_1^* = \frac{\Omega_i^2 L^2 \rho_1}{P_{m0}}, \qquad p_m^* = \frac{p_m}{P_{m0}} \tag{21}$$

where L, Ω_i, P_{m0} are the characteristic scale length, ion gyro-frequency and equilibrium magnetic pressure. The boundary conditions to be satisfied are:

$$\left.\begin{aligned} p_m^* &= 0 \\ Dp_m^* &= 0 \end{aligned}\right\} \quad \text{at } x = 0 \tag{22}$$

and p^*_m and Dp^*_m are bounded as $x \to \infty$.

The system of equations to be solved for the case of zero plasma pressure is different from the system of Eqs. (19)-(22) because, they cannot be derived by taking the limit as pressure goes to zero. The requisite system of equations for the zero plasma pressure case is derived from Eqs. (1 1)-(13) by putting the plasma pressure term (∇p) to zero. Performing normal mode analysis, the system of equations to be numerically solved subject to the boundary condition (22) are written as:

$$DZ_j = \sum_{k=1}^{4} B_{jk} Z_j \quad j = 1,4 \tag{23}$$

where $[z] = [Z_1, Z_2, Z_3, Z_4] = [P;\ , p_m^*, Dp_m^*, q^*]$ (24)

The elements of the matrix B are given in appendix C.

The numerical procedure for solving Eqs. (19), (20) and (21) and the system of equations (23), together with the boundary conditions (22) as an eigenvalue problem by using a two-point boundary value method is descr bed in" Appendix A.

3. Approximate Solutions:

It would be worthwhile to study certain limiting cases of the wave equations (15), (17), and (18) using JWKB approximation before presenting numerical results. Eliminating ρ_1 from equations (15) and (17) with the help of Eq. (18) and neglecting curvature effect we obtain:

$$\left\{\left(\frac{\partial}{\partial t}+U_0\frac{\partial}{\partial x}+\beta\right)\frac{\partial}{\partial x}\right.$$
$$\left.-v_a^{-2}\left(g-U_0\nu_0-c_0^2\frac{\partial}{\partial x}\right)\cdot\left(\frac{\partial}{\partial t}+U_0\frac{\partial}{\partial x}-\eta\nabla^2\right)\right\}p_m$$
$$=\left\{\left(\frac{\partial}{\partial t}+\nu_0\right)\cdot\left(\frac{\partial}{\partial t}+U_0\frac{\partial}{\partial x}+\beta\right)+\frac{N^2}{g}\left(g-U_0\nu_0-c_0^2\frac{\partial}{\partial x}\right)\right\}q \tag{25}$$

$$\left\{k^2\left(g-U_0\nu_0\right)+\left(\frac{\partial}{\partial t}+U_0\frac{\partial}{\partial x}+\beta\right)\frac{\partial}{\partial x}\right\}p_m$$
$$=\left(\frac{\partial}{\partial t}+\nu_0\right)\left(\frac{\partial}{\partial t}+U_0\frac{\partial}{\partial x}-c_0^2\frac{\partial}{\partial x}+\beta+k^2c_0^2+g-U_0\nu_0\right)q \tag{26}$$

It may be interpreted that the perturbations in the magnetic pressure and the particle flux are represented by the left and the right sides of Eqs. (25) and (26) respectively. Also for the sake of

convenience a spatial decay due to density stratification is subtracted out, i.e., we write

$$Q(x,y,t) = Q^*(x)\ \exp(x/2H)\ \exp\ (i\ (k_x x + k_y y - \text{ret})) \qquad (27)$$

In case the magnetic pressure perturbations are negligible as compared to perturbation in particle flux, the right hand sides of Eqs. (23) and (24) with the help of Eq. (27) give

$$\left(-i\omega + \beta + \frac{U_0}{2H}\right)(\nu_0 - i\omega) + \frac{N^2}{g}\left[\, g - U_0\nu_0 - \frac{c_0^2}{2H}\right] = 0 \qquad (28)$$

$$\beta - i\omega + \frac{U_0}{2H} + g + k^2 c_0^2 - U_0\nu_0 - \frac{c_0^2}{2H} = 0 \qquad (29)$$

From Eq. (28) we see that exponentially growing solutions will arise if (U_0 < O , because the equilibrium ionospheric plasma flows in the negative direction of x),

$$\frac{N^2}{9} = - \frac{\nu_0\ \beta + U_0/2H)}{g - U_0\nu_0 - c_0^2/2H} \qquad (30)$$

is sufficiently negative. For a stably stratified ionospheric layer, l/H < 0. The effect of plasma pressure is stabilizing because it decreases the value of N2/g . The effect of radial plasma motion is destabilizing in the numerator whereas it is stabilizing in the denominator. The overall effect depends on the values of l/H and ν_0. Eq. (29) gives purely damped modes for H < 0 and $U_0 < 0$.

In case buoyancy perturbations are negligible as compared to magnetic field perturbations, equating coefficients of p_m from Eqs. (25) and (26) to zero and using Eq. (27), we obtain:

$$\frac{V_a^2}{2H}\left(\beta - i\omega + \frac{U_0}{2H}\right) + \left(g - U_0\nu_0 - \frac{c_0^2}{2H}\right)\left(i\omega - \frac{U_0}{2H} + \eta\left(\frac{1}{4H^2} - k^2\right)\right) = 0 \qquad (31)$$

$$2Hk^2(g - UO\ V.\ ) + \beta - i\omega + UO/2H = 0 \qquad (32)$$

From Eq. (31) we find that in case the effect of inhomogeneity is stronger than the resistive effects, growing solutions will arise if:

$$i\omega = \frac{\left(g - U_0\nu_0 - \frac{c_0^2}{2H} + \frac{V_a^2}{2H}\right)U_0 + \beta V_a^2}{g - U_0\nu_0 - V_p^2/2H} > 0 \qquad (33)$$

and in case inhomogeneity effects are negligible as compared to resi stive effects, $i\omega \rightarrow \eta\ \ k^2$ and the system is stable, Equation (32) gives unstable modes if:

$$U_0 < -2H\left(\beta + 2Hk^2\left(g - U_0\nu_0\right)\right) \qquad (34)$$

which will be satisfied if $\beta + 2Hk^2(g - U_0\ \nu_0) > 0$. The instability condition for a stagnant plasma in the vicinity of the cometary ionopause is $\beta + 2Hk\ \ 2_g > 0$.

Iv. Computational Results with Application to the Comet Halley:

The non-dimensional background physical quantities are given by

$$\beta \equiv 0.1\ /\ (X + X_0) \qquad (35a)$$

$$X = \frac{r - r_0}{L}, \qquad X_0 = \frac{r_0}{L} \tag{35b}$$

$$\nu_0 = \nu + \frac{\beta}{2} \tag{35c}$$

$$v_a^2 = \Omega_i^2 L^2 \cdot X_1 (X_m \cdot X_{ln} \cdot v_{am}^2) \tag{35d}$$

$$N^2 = g / (X_1 \cdot X_m \cdot X_{ln}) \tag{35e}$$

$$g = g / (L^2 \Omega_i) \tag{35f}$$

$$X_1 = (X + X_0) / X_m , \qquad X_{ln} = 1 + 2 \ln X_1 \tag{35g}$$

$$\eta^* = \eta / (L^2 \Omega_i) , \qquad U_0^* = U_0 / (L \Omega_i) \tag{35h}$$

where V_{am}^2 is the square of the characteristic Alfven velocity at the exterior of the cometo-sheath. V_a^{-2}, N^2, and β are shown in Figs (1a,b). η^* and U_0^* are non-dimensional plasma resistivity and plasma velocity respectively. Ω_i is the Larmor frequency of water group ion and L is the characteristic length.

The plasma parameters for numerical computation for the comet Halley are: r_m = 8400 km, and r_0 = 4600 km, the distances from the nucleus at which the magnetic field has maximum and minimum values ($B_{max} \cong$ 50 nT, B_{min} = O). They are used to obtain the profile of the magnetic field in the sheath region. N_n, the number density of neutrals $\cong$ 5.5 x 10^6 cm^{-3} with the total sublimation rate Q $\cong$ 6.9 x 10^{29} molecule s^{-1} and $V_n \cong$ 0.9 km s^{-1}, ν the ion neutral collision frequency $\cong$ 6 x 10^{-3} s^{-1}, α the dissociative recombination rate taking

account of the dependence on ion and neutral densities (Mendis et al., 1985) is $\cong 7.0 \times 10^{-7} \sqrt{300/T_e}\ cm^3\ s^{-1}$, where T_e is the electron temperature. For T_e - 300 K (Ip et. al., 1987), α comes out to be 7 x $10^{-7}\ cm^3\ s^{-1}$ and for T_e - 2000 K , α comes out to be 1.565 x 10^{-7} $cm^3\ s^{-1}$ (0.2236 times smaller than that for T_e = 300 K), Decrease in α implies decrease in β. Assuming photochemical equilibrium Eq. (5) gives $n_{i0} \sim 3000\ cm^{-3}$ for δ -- $10^{-6}\ s^{-1}$.

Using the above parameters, we have calculated the eigenvalues and the eigenfunctions with the help of the method described in Appendix A for two values of η, the plasma resistivity taken from Cravens, (1989) and two values of sound velocity taken from Flammer et al., (1991). TABLE I shows growth rate-wave number, (ω_i, k) relation for the nondimensional resistivity, $\eta^* = 1.0$ (5 km 2/s) and sound velocity equal to zero (no plasma pressure) and plasma velocity equal to -2 km/s. TABLE 11 shows growth rate-wave number, (ω_i, k) relation for the nondimensional resistivity, η^* = 1.0, 0.5 (5, 2.5 km^2/s) sound velocity equal to 1.0 and $\sqrt{2}$ km/s and plasma velocity equal to -0.2 km/s. Flammer et al., (1991) have taken a plasma velocity of 5 km/s at the right end of the simulation box ' which is about 13700 km from the cavity surface. The plasma velocity decreased linearly to zero at the ionopause boundary. We have performed the stability analysis of ionospheric ayer of about 1000 km thickness adjacent to the cavity surface, in which the plasma has a very slow motion ($U_0 < 2$ km/s). We have thus chosen a small radial velocity to ascertain its effect on the stability. Flammer et al., (1991) have taken plasma beta equal to 0.332 and V_A, the

Alfven velocity of about 3 km/s, which gives a sound velocity of the order of 1 km/s. It was a hard task to compute eigenvalues and as such the equations were solved only for a limited number of cases as given in the tables. It can be seen from the tables that we find growth rates for perturbations of wavelengths ranging from 200 km to 2000 km. However, the growth rates change by an inappreciable amount by a change in the wavelength of perturbations. It is also noted that increase in plasma velocity reduces growth rates. It is found that the growth rates of linear stability decrease with increasing sound velocity. It can be seen from the Tables that growth rates are larger for smaller resistivity, i.e., the resistivity has a stabilizing effect. Thus, it is concluded that the plasma resistivity, pressure and radial plasma motion have stabilizing effect on the cometo-sheath but are unable to quench the instability completely. The thickness of the ionopause transition layer is only ~ 25 km (Neubauer, 1988) and it was not possible to obtain solution of equations in this layer due to the singularity in the magnetic field (B=O at the ionopause boundary). The deeper into the ionospheric layer, the growth rates become larger due to the fact that hydromagnetic counterpart of square of the Brunt-Vaisala (Eckart, 1960) frequency, N^2 (shown in Fig. (lb)), is negative and increases sharply close to the ionopause transition layer.

We have obtained growth rates for the Halley cometo-sheath, a layer of about 1000 km thickness neglecting plasma pressure for wavenumbers ranging from k=0.3 t0 k=5. The corresponding wavelengths lie in the range from 125 km to 2000 km. In the case of

the cometosheath with no plasma pressure, the thickness of the ionospheric layer adjacent to cavity surface is taken as 1000 km and the characteristic length, L = 100 km whereas the thickness of the layer and the characteric length with plasma pressure are taken as 500 km and 50. We have estimated the range of τ_c/τ_i to explore the possibility of convection of perturbation well downstream into the ionopause. Here, $\tau_c = d / V_g$, is convection time for the perturbations to penetrate through a distance d and Vg = ω_r / k, is the group velocity; $\tau_i = 1/\omega_i$, is the characteristic time for the instability to grow. The cometo-sheath would be effectively stable if $\tau_c/\tau_i \leq 1$ evenwhen $\omega_i > 0$, and unstable if $\tau_c/\tau_i >> 1$.

Our calculations show that τ_c/τ_i = d k L ω_i /(L ω_r), varies from 20 to 35 for d = 1000 km, ω_i / ω_r = 0.7 (from Table I) and d/L = 10 for k *= k L varying from 3 to 5 and characteristic length, L = 100 km. This value of appears to be sufficient for the effective penetration of magnetic field perturbations into the cavity surface. For the case of cometo-sheath including the effect of plasma pressure τ_c/τ_i varies from 8 to 15 for

ω_i / ω_r =0.5 and kL = 2.0 and d/L = 10, for d = 500 km and L = 50 km. The value of τ_c obtained by Ershkovich et al., (1989) was of the order of 2000 s. Taking this value of τ_c and the numerically obtained value of $1/\tau_i$ = 0.006, τ_c/τ_i comes out to be of the order of 12 which appears to be sufficient for the convection of perturbations well into the cavity surface, Thus we conclude that the cometary ionopause cannot be at rest and ripples must appear as shown in Fig, (1c). Motion of the Halley ionopause seems to have been observed:

according to Neubauer (1 987), Halley ionopause seemed to have strong ripples with a wavelength of several hundred kilometers.

It would be of interest to see how the various perturbations vary in the inner cometo-sheath. Figs. (2a,b) and (3a,b) show the real and imaginary parts of the eigenfunctions viz., ρ_{1r}, P_{1i} and q_r, q_i (real and imaginary parts of perturbations in density and particle flux) for certain wave numbers for cold plasma for $\omega_r = 0.0$, $\eta^* = 1.0$, and $U_0 = O$ as a function of distance in km from the ionopause cavity boundary, Figs, (2a,b) show that perturbation in density is maximum at the ionopause. Figs. (3a,b) and (5a,b) show that the perturbation in plasma flux is also maximum at the ionopause. The effect of plasma pressure changes this result, i.e., the density perturbations start decreasing after attaining a maximum at about 100 km from the ionopause as can be seen from Figs. (6a, b). This results due to the stabilizing effect of plasma pressure, Figs. (4a,b) and (5a,b) show the eigenfunctions p_{mr}, p_{mi} (p_{mr}, P_{mi} are the real and imaginary parts of perturbations in magnetic pressure) and q_r, q_i for the same parameters but $U_0 = 2$ km/s as a function of distance from the ionopause for certain wave numbers. Figs. (6a,b) and (7a,b) show the eigenfunctions ρ_{1r}, ρ_{1i} and p_{mr}, p_{mi} for certain wave numbers for $\eta^* = 0.5$, sound velocity $c = \sqrt{2}$ km/s and $U_0 = O$, Figs. (4a,b) and (7a,b) show that perturbation in magnetic pressure vanishes at the ionopause which was imposed as a boundary condition for the solution of wave equations.

5 . Conclusions:

We have investigated the linear MHD stability of the cometary inner sheath of 1000 km thickness for a cold plasma and 500 km thickness for a hot plasma surrounding the diamagnetic cavity of the comet Halley bounded by the ionopause on the inner side including the effects of resistivity, plasma pressure and motion by numerically solving the equations governing the stability and also by discussing certain limiting cases of the wave equations, The thickness of the cometo-sheath for a cold and warm plasma was taken differently for the convenience of numerical computation. The equations governing the stability are solved numerically for certain parameters for the comet Halley by using a two-point boundary value method. Although, the two-point boundary value method precludes the study of the stability of the critical layer of 25 km thickness due to the singularity of solutions as the magnetic field goes to zero at the boundary of the transition layer, the present work is a step forward in that it presents numerical solutions and includes the effects of finite resistivity and radial plasma motion on the stability of the cometo-sheath which were not considered in previous papers (Ershkovich et al., 1989; McKenzie et al., 1990; Srivastava et al., 1992; Ershkovich and Israelevich, 1992). The eigenvalues are given in tables I and 11 and the eigenfunctions are shown in Figs (2)-(7). Certain limiting cases of the wave equations have also been discussed. We have obtained growth rates for disturbances of wavelengths ranging from 125 km to 2200 km (125 km to 2200 km for a cold plasma and 200 km to 1050 km for a warm plasma). We

have also estimated τ_c/τ_i where τ_c is the convection time for the perturbations to be convected well downstream and τ_i is the characteristic time for the amplitude to grow and found that it ranges from 10 to 20 or even higher which may be sufficient for the instability signatures to penetrate the boundary. The effects of photoionization, recombination, plasma pressure, and resistivity were found stabilizing but the instability still persisted. The slow plasma motion included in the analysis resulted in the stabilization of the cometo-sheath since perturbations are convected downstream with the plasma bulk velocity before growing substantially.

The main conclusions of the study are:

1. It is shown that the magnetic field structure resulting from the balance between the magnetic stresses and the ion-neutral drag force in the cometary inner sheath is unstable to disturbances of wavelengths ranging from 100 km to 2200 km for the cold plasma and from 200 km to 1100 km for a warm plasma(sound speed of about a kilometer/s).

2. The inclusion of plasma pressure in the stability analysis results in the stabilization of the cometosheath. The instability rates for the cold plasma are very much larger than those for a plasma with pressure.

3. Effects of recombination and plasma resistivity are stabilizing but are unable to quench the instability completely. Growth rates are reduced by the increase in resistivity and recombination rate.

4. The slow plasma motion included in the analysis reduces growth rates and results in the stabilization of the cometo-sheath since perturbations are convected downstream with the plasma bulk velocity $-U_0$ before growing substantially. An estimate of τ_c/τ_i shows that it lies in the range 10 to 20(or even higher) which appears to be sufficient for the effective penetration of the magnetic field perturbations into the cavity surface. Thus we conclude that the cometary ionopause cannot be at rest and ripples must appear as shown in Fig. (1c). Motion of the Halley ionopause has been confirmed by observations: according to Neubauer (1987), Halley ionopause seemed to have strong ripples with a wavelength of several hundred kilometers.

5. The main cause for the instability of the cometosheath is that the square of Brunt-Vaisala, N^2 is negative and increases sharply close to the ionopause transition layer (25 km thickness).

6. Increase in the neutral production rate causes increase in plasma density which results in a higher value of β which has stabilizing effect. It is thus conjectured that the inactive comets at large distances from the sun, say 2-3 A. U., where productivity is less should be highly unstable,

7. It is reasserted (we concluded the same in our previous paper Srivastava et al., 1993) that the comets at larger distances, say 2-3 A. U., where the productivity of neutrals is less will be much more unstable because the total sublimation rate, Q, increases with the

number density of neutral molecules. As Q increases, ν_0 increases due to the increase in β. Increase in β results in the reduction of growth rates.

A nonlinear stability analysis of the Halley ionopause and the adjacent layer would be certainly helpful in understanding the the structure of the inner sheath.

Appendix A

Equations (19), (20), and (21), and the system of equations (23) together with the boundary conditions (20) are solved numerically as an eigenvalue problem by using a two-point boundary value method. They are written in the form:

$$DZ_j = \sum_{k=1}^{4} A_{jk} Z_j \quad , \qquad j = 1, 4, \qquad k = 1, 4 \tag{A1}$$

$$Z_3 = p_m^* = 0$$
$$Z_4 = Dp_m^* = 0 \qquad \text{at } x = 0 \tag{A2}$$

and p_m^* and Dp_m^* are bounded as x tends to infinity ($x = x_e$) where, A_{jk} is the coefficient matrix, and $D = \frac{d}{dx}$. $x = x_e$ defines the exterior edge of the boundary layer.

Outside the boundary layer, solutions of Eqs. (A1) are written in the form

$$Z_j = \sum_{k=1}^{4} C_{jk} \exp(\lambda_k x) \quad , j = 1, 2, 3, 4 \tag{A3}$$

where C_{jk} is the fundamental matrix. The characteristic roots of the matrix A_{jk} are λ_1, λ_2 and $-\lambda_3, -\lambda_4$ which are obtained numerically. As the solutions are bounded as $x \to \infty$, the eigenvalues with positive real parts viz., λ_1, λ_2 must be

discarded, thereby leaving only two linearly independent exponentially decaying solutions.

The eigenvalues and the eigenfunctions are obtained with the help of a computer code for solving two-point boundary value problems (Scott and Watts, 1977). This method of evaluating eigenvalues and eigenfunctions has been widely and successfully used (Nayfeh, 1981; Floryan and Saric, 1982, Srivastava and Dallmann, 1987 and references therein). For fixed values of background physical parameters and chosen values of ω_r, and k an estimate for ω_i is made. The known solutions at x = x_c are used as the initial conditions and the integration is performed from x = x_c to zero. In case the computed solution does not satisfy the boundary conditions at x = 0, ω_i is incremented by using a Newton-Raphson scheme, The process is repeated until the boundary conditions at x = O are satisfied to within a specified accuracy. The eigenvalues of the adjoint problem are the same as those of the basic problem,
The boundary conditions at x = x_c are obtained by writing Eqs. (Al) in the form:

$$DZ = A_{\infty} Z \qquad \text{(A4)}$$

where A_{∞} is the matrix for x = x_c. The characteristic roots with positive rea parts lead to growing solutions. Hence, the eigenvalues with positive real parts must be discarded, thereby leaving only two linearly decaying solutions. To achieve this, we consider the general

solution obtained by superposition of fundamental solutions. We write,

$$Z = C\, b \tag{A5}$$

The fundamental matrix C is a matrix containing no terms in x. Inverting system (A5), we obtain

$$C^{-1} Z = b \tag{A6}$$

The asymptotic boundary conditions require that b = O. By reducing matrix A_∞ to a Jordan canonical form with the help of a similarity transformation J = P-1 A_∞ P, and by using the concept of adjoint system, we obtain the boundary conditions for the adjoint system as

$$S^* Z^* = 0 \qquad \text{at } x = x_e \tag{A7}$$

where S* consists of the last row of P^T. Here, P is the similarity transformation. matrix and PT is its transpose.

The boundary conditions at x = XC for the basic system are

$$T\, z = o \tag{A8}$$

where T consists of the last row of P^{*T}. P* is the complex conjugate of P and P^{*T} is its transpose.

Appendix B

The coefficients of the differential equations (17) and (18) are :

$a_{11} = 0, \qquad a_{12} = 0, \qquad a_{13} = 0, \qquad a_{14} = 1$

$$a_{21} = k^2 + \left(\frac{\partial}{\partial t} + \nu_0\right)\left(\frac{\partial}{\partial t} + P\right) / c: + V_a^2 \left| \frac{\partial}{\partial t} + \beta + \frac{N^2}{g} \frac{(g - U_0\nu_0)}{\left(\frac{\partial}{\partial t} + \nu_0\right)} \right| ,$$

$$/ \ (\eta c_s^2 \ )$$

$$a22 = \ (\ g + U_0\frac{\partial}{\partial t} \ ) \ / \ c_s^2 + V_a^2 \left(U_0 - \frac{N^2}{g} \frac{:_{s_s}^2}{\left(\frac{\partial}{\partial t} + \nu_0\right)} \right) / (\eta c_s^2 \ )$$

$$a_{23} = - \frac{\partial}{\partial t} / \ (\text{Tic: })$$

$$a_{24} = - \left(U. + \frac{N^2}{g} \frac{V_a^2}{\left(\frac{\partial}{\partial t} + \nu_0\right)} \right) / (\eta c_s^2)$$

$$a_{31} = 0, \qquad a_{32} = O, \qquad a_{33} = O, \qquad a_{34} = 1,$$

$$a_{41} = - \frac{V_a^2}{\eta} \left(\frac{\partial}{\partial t} + \beta + \frac{N^2}{g} \frac{(g - U_0\nu_0)}{\left(\frac{\partial}{\partial t} + \nu_0\right)} \right)$$

$$a_{42} = - \frac{V_a^2}{\eta} \left(U_0 - \frac{N^2}{g} c_s^2 \frac{1}{\left(\frac{\partial}{\partial t} + \nu_0\right)} \right)$$

$$a_{43} = k^2 + \frac{1}{\eta} \frac{\partial}{\partial t} , \qquad a_{44} = \frac{1}{\eta} \left(U_0 + \frac{N^2}{g} \frac{V_a^2}{\left(\frac{\partial}{\partial t} + \nu_0\right)_{\prime\prime}} \right)$$

$$\frac{a}{\partial t} = -\imath\omega$$

Appendix C

The elements of the matrix B are :

$b_{11} = -Rh/Rhd$, $b_{12} = -\frac{i\omega}{V_a^2}\frac{1}{Rhd}$

$b_{13} = \frac{U_0}{V_a^2}\frac{1}{Rhd}$, $b_{14} = -\frac{N^2}{g}\frac{1}{Rhd}$

$b_{21} = 0$. $b_{22} = b_{24}$, $b_{23} = 1$

$b_{31} = (-i\omega + V.)(-i\omega + \beta) + (g - i\omega U_0) . Rh/Rhd$

$b_{32} = k^2 - i\omega (g - i\omega U_0) / (V_a^2 . , hd) - \frac{Rhd}{(1+Rhd)}\frac{d}{dx}\frac{2}{R}$

$b_{33} = (g - i\omega U_0) U_0 / (V_a^2 . Rhd) - \frac{2Rhd}{R(1+Rhd)}$

$b_{34} = -\frac{N^2}{g}\frac{(g - i\omega U_0)}{Rhd}$

$b_{41} = i\omega - \beta - \frac{U_0 R_h}{Rhd} . \frac{1}{(\nu_0 - i\omega)}$

$b_{42} = \left(\frac{i\omega U_0}{V_a^2, Rhd} - k^2 + \frac{1}{Rhd}\frac{d}{dx}\frac{2}{R}\right) / (\nu_0 - i\omega)$

$b_{43} = \left[\frac{2}{R''}\frac{-1}{Rhd} - \frac{U_0^2}{V_{a''}^2 Rhd}\right] 1 / (V_1 - i\omega)$

$b_{44} = \frac{N^2}{g}\frac{U_0}{Rhd}\frac{1}{(\nu_0 - i\omega)}$

where

$R_h = \beta - i\omega + \frac{\eta}{V_a^2}(\beta - i\omega)(\nu_0 - i\omega)$

$Rhd = U_0 + \frac{g\eta}{V_a^2} - \frac{\eta U_0}{V_a^2} i\omega$

Acknowledgements:

Portions of this work were done at the Jet Propulsion Laboratory, California Institute of Technology under contract with the National Aeronautics and Space Administration. Also, this work was performed during the period Krishna M. Srivastava held a senior Resident Research Associateship administered by the National Aeronautics and Space administration through the National Research Council. Useful discussions with M. Neugebauer and K, Flammer are thankfully acknowledged. Thanks are also due to R, Sakurai for reading the manuscript. We thank the referees for useful comments.

References:

Balsiger, H., et al., Ion composition and dynamics at comets, *Nature*, 321, 330, 1986.

Brunt, D. 1941, in *Physical and Dynamical Meteorology (Cambridge: Cambridge University Press).*

Cravens, T. E., Cometary plasma boundaries, *Adv. Space Res., 9, 293, 1989.*

Cravens, T. E., and Korosmezey, A., Vibrational and rotational cooling of electrons by water vapor, *Planet. Space Sci., 34, 961, 1986.*

Eckart, C. 1960, in *Hydrodynamics of Oceans and Atmospheres (New York: Pergamon), 1960.*

Ershkovich, A. 1., and D. A. Mendis, Effects of interaction between plasma and neutrals on the stability of the cometary ionopause, *Ap. J., 302, 849, 1986.*

Ershkovich, A. I., K. R. Flammer and D. A. Mendis, Stability of the sunlit cometary ionopause, *Ap. J., 311, 1031, 1986.*

Ershkovich, A. I., and Flammer, K. R., Nonlinear stability of the dayside cometary ionopause, *Ap. J.*, 328, 967, 1988.

Ershkovich, A. I., et al., Stability of a cometary ionosphere/ionopause determined by ion-neutral friction, *Ap. J., 344, 932., 1989.*

Ershkovich, A. 1. and P. L. Israelevich, On the convective instability of the cometary ionosphere, submitted to *Ap. J.*, 1992

Eviatar, A. , and B. E. Goldstein, A unidirectional model of comet ionosphere structure, *J. Geophys. Res., 93,1759, 1988.*

Flammer, K. R., N. Omidi and K. B. Quest, The structure of a tangential discontinuity: Application to the cometary ionopause, *Geophys. Res.*

Lett., 18, 369, 1991.

Floryan, J. M., and Saric, W. S., Stability of boundary layer flow on concave surface, *AIAA J. 20, 316, 1982.*

Hasam, A. B. and J. D. Huba, Magnetohydrodynamic equations for systems with large Larmor radius, *Phys. Fluids,* 31, 318, 1988.

Ip, W.-H., and W. I. Axford, Theories of physical processes in the cometary comae and ion tails, *in* Cornets, *ed. L. L. Wilkening (Tucson: University of Arizona Press), 588, 1982.*

----------, *The* formation of a magnetic field-free-cavity at comet Halley, *Nature, 325, 418, 1987.*

----------, *The* Plasma, *in Physics and Chemistry of Comets, ed. W. F. Huebner (Springer Verlag, Berlin), 1990, 177.*

McKenzie, J. F., et al., Stability of a cometary ionosphere /ionopause including pressure effects, *Ap. J.,* 360, 275, 1990.

Mendis, D. A., Houbis, H. L. F., and Marconi, M. L., The physics of comets, *Fund, Cosmic Phys., 10, 1, 1985,*

Nayfeh, A. H., Effect of streamwise vortices on Tollmien-Schlichting waves, *J. Fluid Mech., 107, 441, 1981.*

Neubauer, F. M., et al., First results from the Giotto magnetometer experiment at comet Halley, *Nature, 32], 352, 1986.*

Neubauer, F. M., Giotto magnetic field results on the boundaries of the pile-up region and the magnetic cavity, *A. & A.,* 187, 73, 1987.

Neubauer, F. M., The ionopause transition and boundary layers at comet Halley from Giotto magnetic field observations, *J. Geophys. Res.,* 93, 7272, 1988,

Scott, M. R., and H, A. Watts, Numerical method for the solution of a two-point linear boundary value problem, *SIAM J. Numer. Anal., 14,*

40, 1977.

Srivastava, Krishna M., and Dallmann, U. , Effect of streamwise vortices on Tollmien-Schlichting waves in growing boundary layers, *Phys. Fluids, 30, 1005, 1987.*

Srivastava, Krishna M., et al., Numerical solution of wave equations for the stability of the cometo-sheath, *Ap. J., 409, 1993 (in Press).*

Fig, (6a,b) show the real and imaginery parts of perturbation in density ρ_{ir} and ρ_{ii} against distance in km from the ionopause for k= 0.3 and 0.4 and U_0=0.0 , the sound velocity, $c_S = \sqrt{2}$ km s^{-1} and η*=1 .0.

Fig. (7a,b) show the real and imaginery parts of perturbation in particle flux $\rho_0 u_{xr}$ and $\rho_0 u_{xi}$ against distance in km from the ionopause for k= 0.3 and 0.4 and U_0=0.0 , the sound velocity, $c_S = \sqrt{2}$ km s^{-1} and η*=1.

Table 1, (ω_i, k) Relation with no Plasma Pressure
L, the characteristic scale length = 100 km

kL	ω_i / Ω_i, the growth rates multiplied by 10		
	$\omega_r / \Omega_i = 0.0$	ω_r / Ω_i '0.1	ω_r / Ω_i '0.1
	$\eta^* = 1.0$	$\eta^* = 1.0$	$\eta^* = 1.0$, $U_0 \cong -2.0$ km/s
	($\eta = 5$ km^2 S-1)		
0.3	**0.3710**	**1.76**	
0.4	**0.3627**	**1.47**	
0.5	**0.3569**	**1.18**	
0.6	**0.3510**	**0.93**	
0.7	**0.4348**	**0.88**	0.065
0.8	0.3467	0.83	0.067
0.9	0.3390	0.81	0.069
1.0	0.3326	0.77	0.065
1.1	0.3319	0.75	
1.2	0.3317	0.70	
1,5	0.3320	0.70	
1.8	0.3340	0,69	
2.0	0.3360	0.69	
2.5	0.3392	0.67	
5.0	0.3469		

Table 11. (ω_i, k) Relation with Plasma Pressure
L, the characteristic scale length = 50 km

$\omega_r / \Omega_i = 0$

kL	ω_i / Ω_i, the growth rates multiplied by 10^2				
	C_s=1 km/s	C_s=$\sqrt{2}$km/s	C_s=1 km/s	C_s=$\sqrt{2}$ km/s	C_s=1 km/s
	η^*=1.0 (η = 5 km^2 S-l)	η^*=1.0	η^*=0 .5 (η = 2.5 km^2 S-l)	η^*=0 .5	η^*=1.0 UO=–O.2 km/s
0.3	0.1640	0.1600	0.1680	0.1617	
0.4	0.1710	0.1836	0.1810	0,1873	
0.5	0.2230	0.2103	0.2360	0.2254	
0.6	0.2711	0.2369	0.2879	0.2685	0.212
0.7	0,3120	0.2748	0.3381	0.3104	0.245
0.8	0.3450	0.3034	0,3838	0,3486	
0.9	0,3621	0.3275	0.4264	0,3838	
1.0	0.3850	0.3471	0.4633	0.4149	
1.1	0.’4120	0.3621	0.4900	0.4424	
1.2			0.5284	0,4664	
1.3			0.5410	0.4871	
1.4			0.5647	0.5045	
1.5				0.5190	
1.6				0.5305	

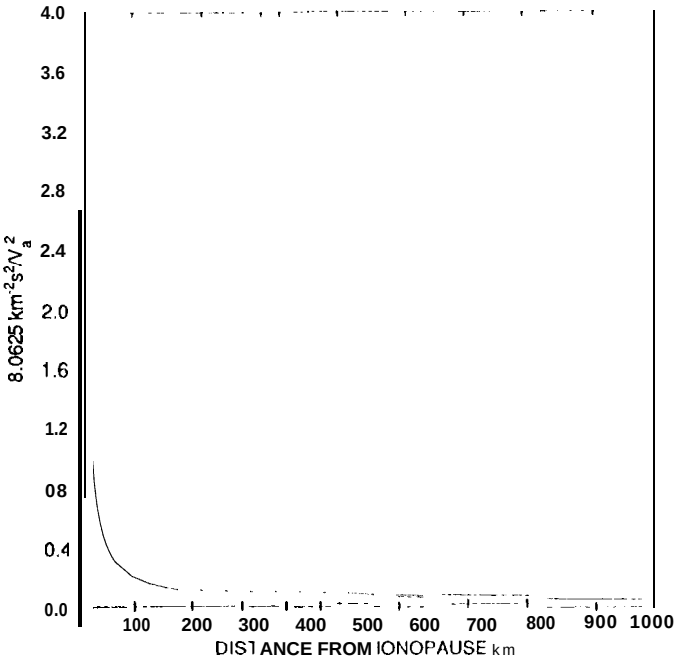

FIGURE 1a

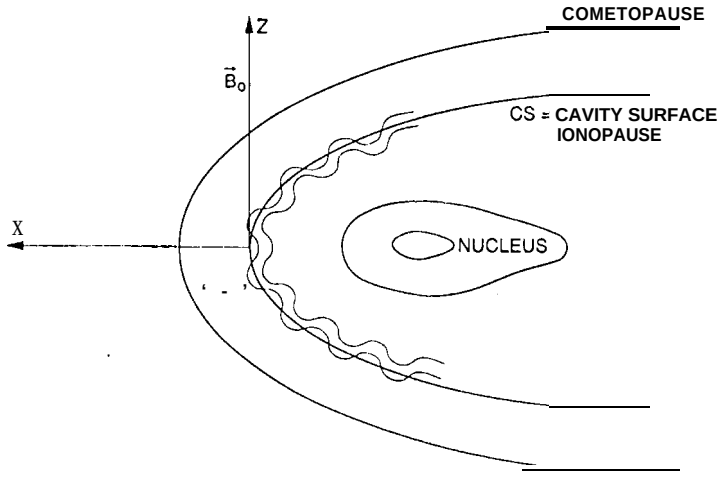

Fig. 1c

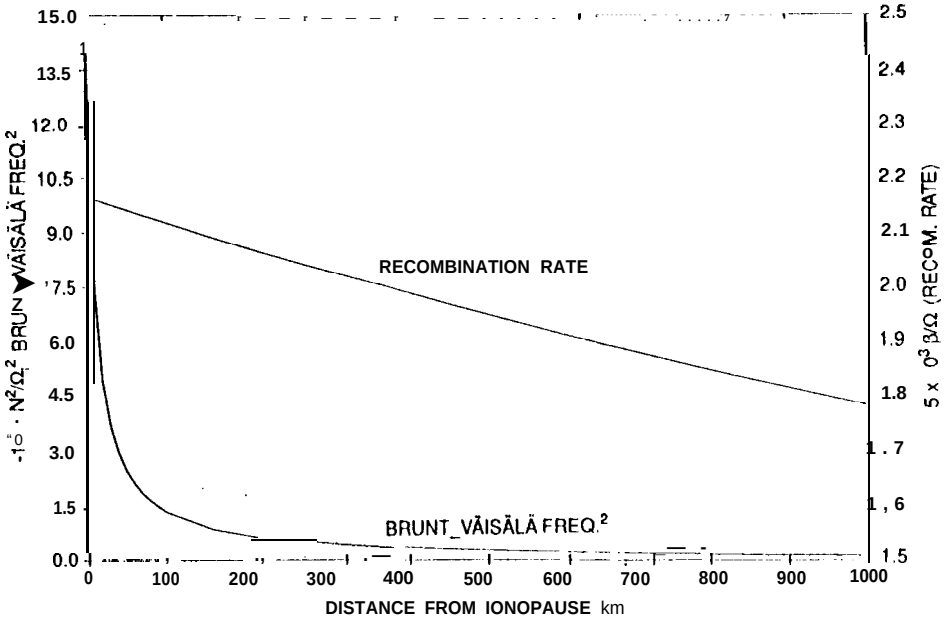

FIGURE Ib

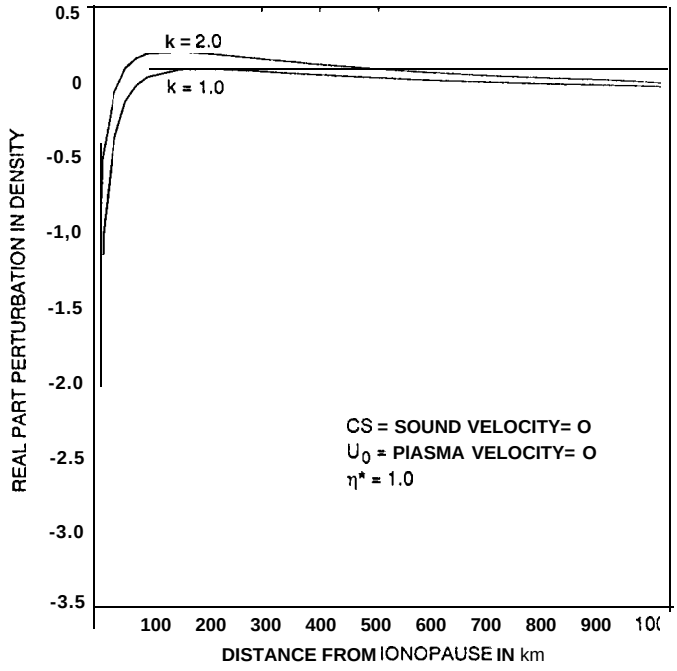

Fig. 2a

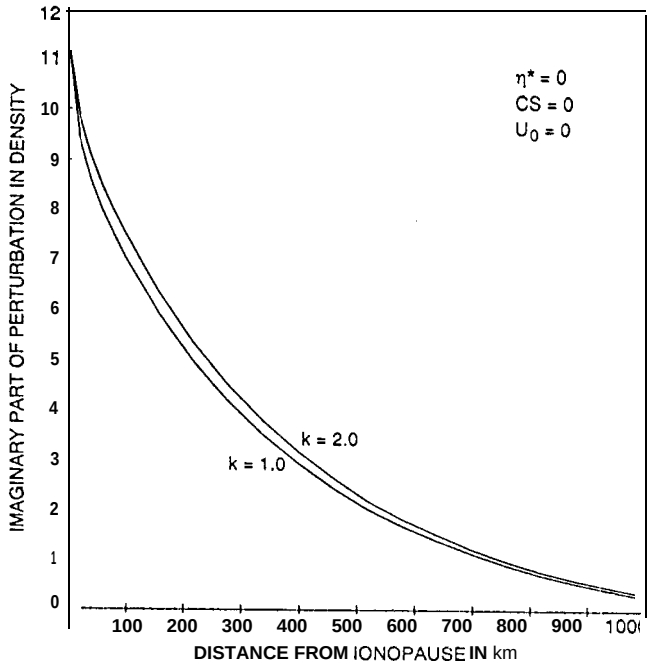

Fig. 2b

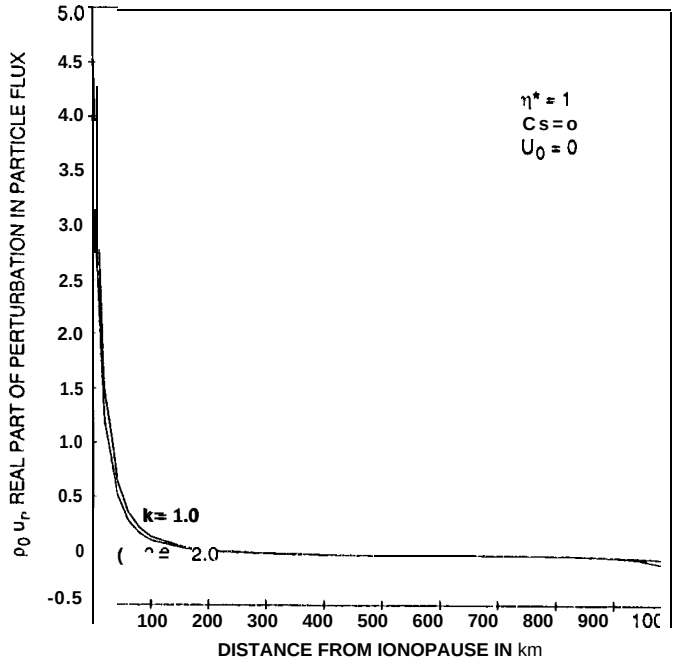

Fig. 3a

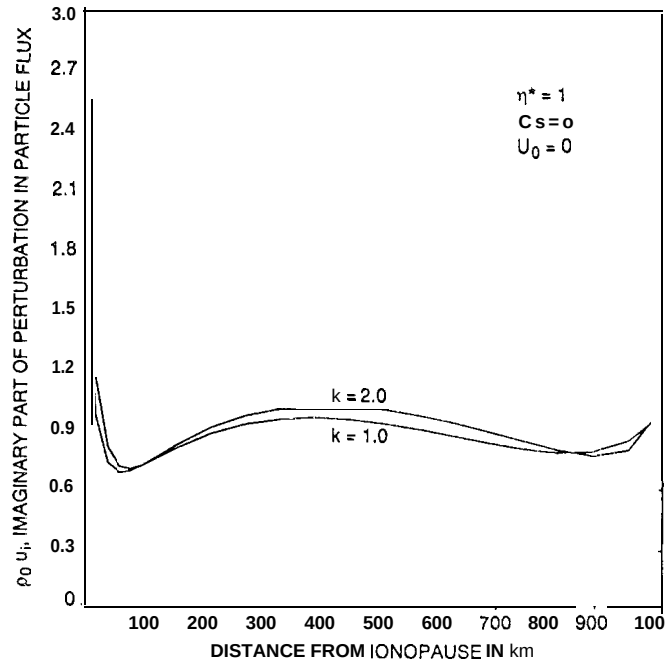

Fig. 3b

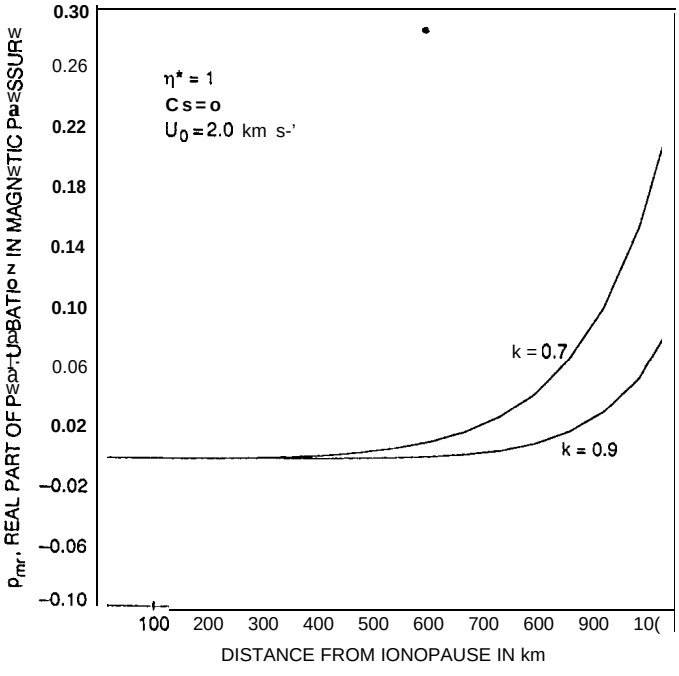

Fig, 4a

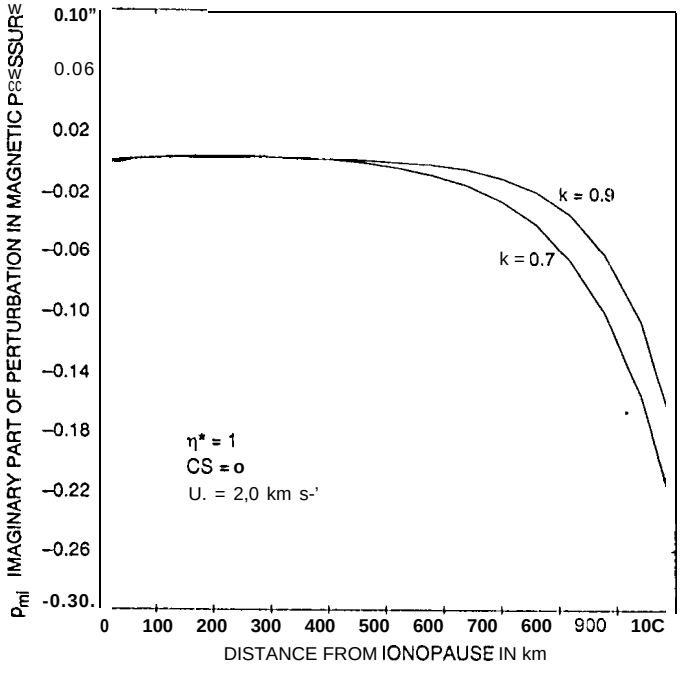

Fig, 4b

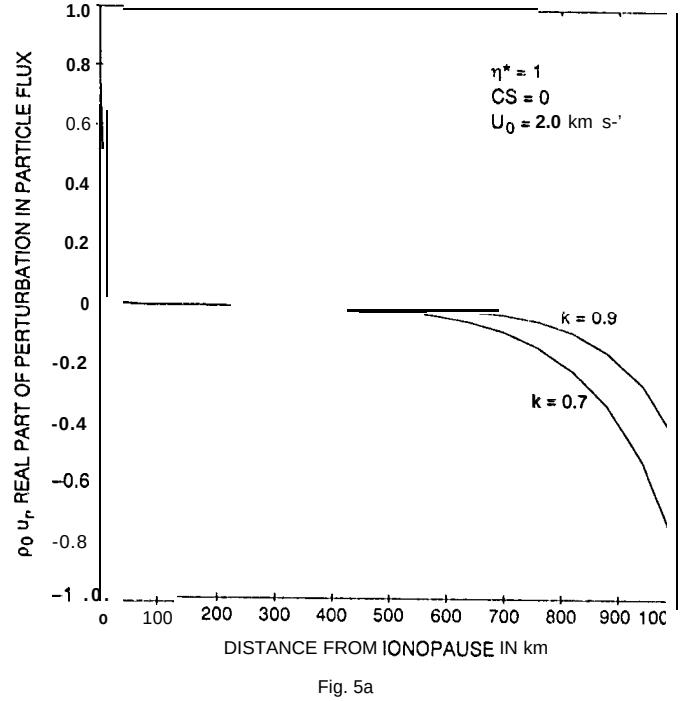

Fig. 5a

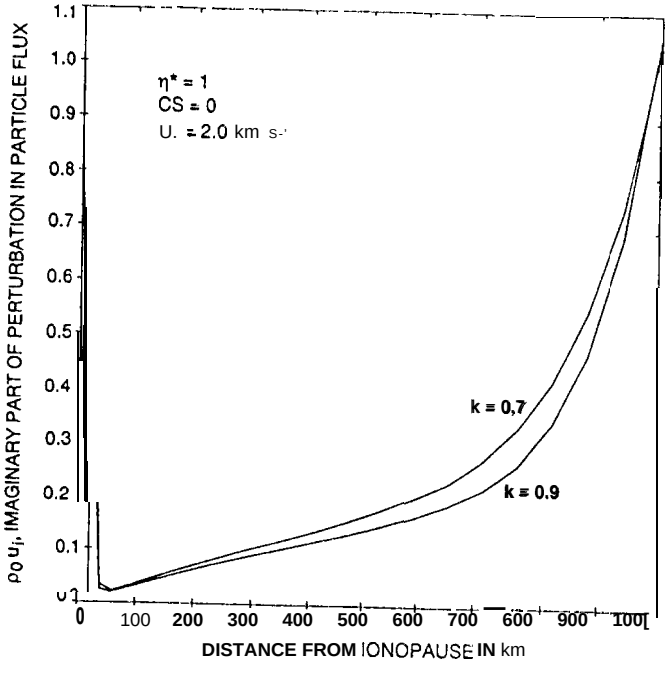

Fig. 5b

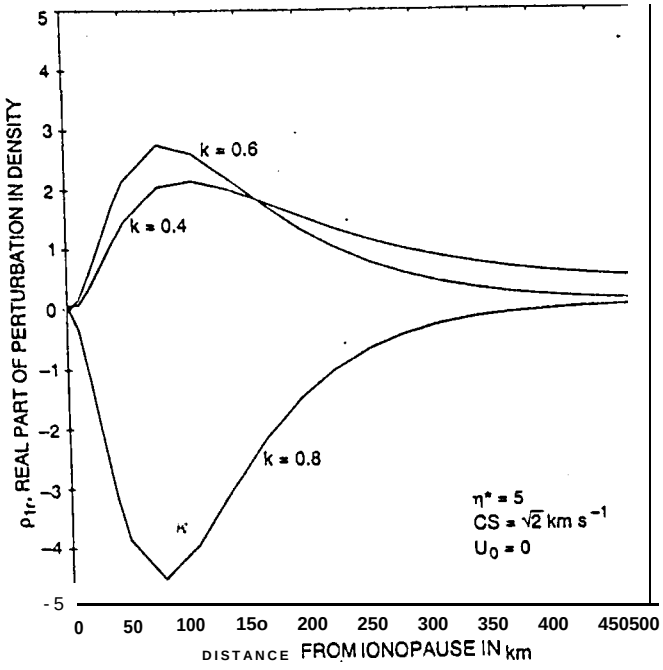

Fig. 6a

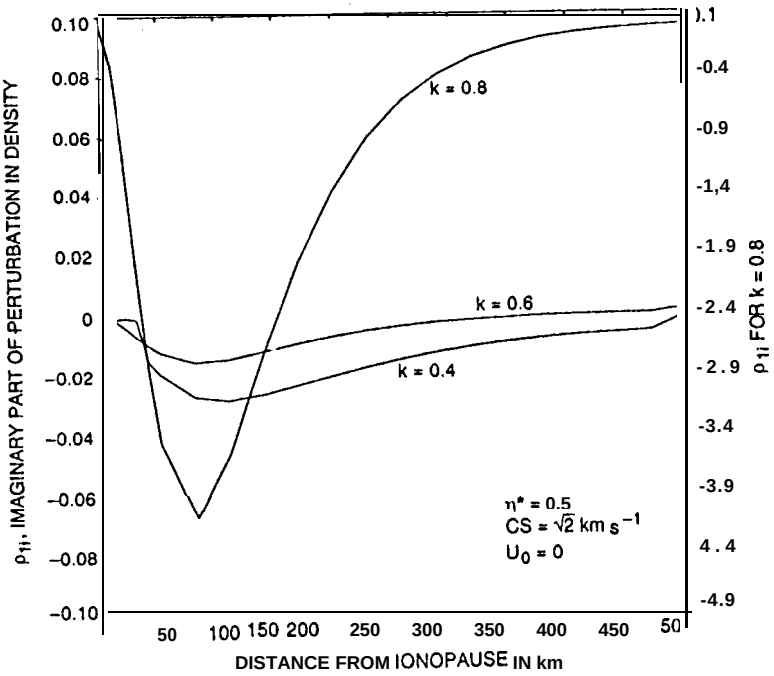

Fig. 6b

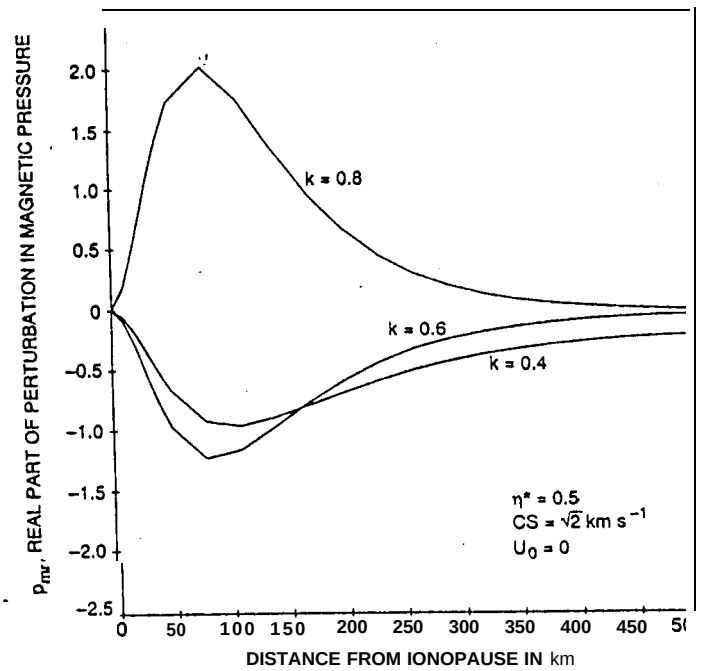

Fig. 7a

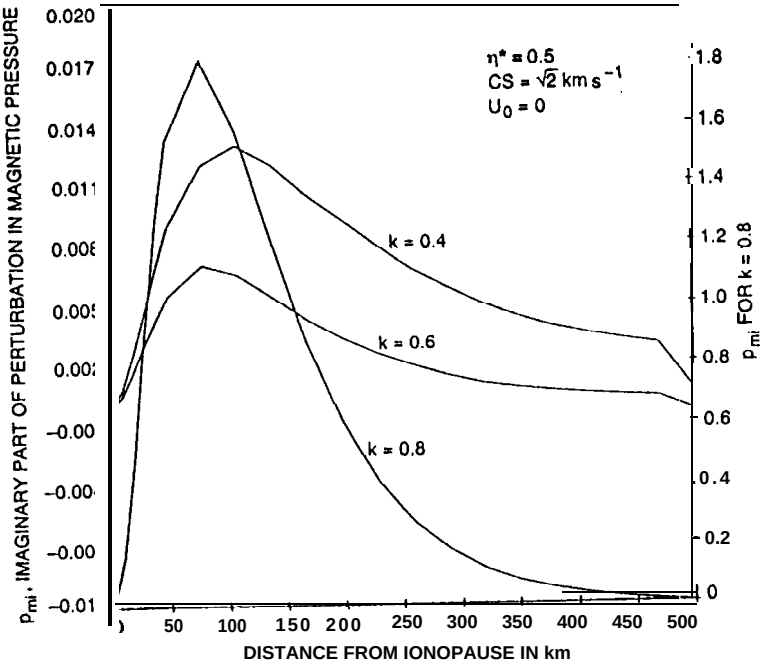

Fig. 7b